Chinese Chemical Letters 34 (2023) 107497

Contents lists available at ScienceDirect

Chinese Chemical Letters

journal homepage: www.elsevier.com/locate/cclet

In situ crosslinking of polyoxometalate-polymer nanocomposites for robust high-temperature proton exchange membranes

Gang Wang[a], Jialin Li[b], Haibin Li[a], Haibo He[a], Liang Zhai[a], Xiang Li[a], Tingting Li[a], Chengji Zhao[b], Lixin Wu[a], Haolong Li[a,b,*]

[a] State Key Laboratory of Supramolecular Structure and Materials, College of Chemistry, Jilin University, Changchun 130012, China
[b] Key Laboratory of High Performance Plastics, Ministry of Education, College of Chemistry, Jilin University, Changchun 130012, China

ARTICLE INFO

Article history:
Received 14 April 2022
Revised 30 April 2022
Accepted 7 May 2022
Available online 11 May 2022

Keywords:
Polyoxometalates
Comb copolymers
Self-assembly
In situ crosslinking
Proton exchange membranes

ABSTRACT

The most practical high-temperature proton exchange membranes (PEMs) are phosphoric acid (PA)-doped polymer electrolytes. However, due to the plasticizing effect of PA, it is a challenge to address the trade-off between the proton conductivity and the mechanical performance of these materials. Here, we report an effective strategy to fabricate robust high-temperature PEMs based on the *in situ* electrostatic crosslinking of polyoxometalates and polymers. A comb copolymer poly(ether-ether-ketone)-*grafted*-poly(2-ethyl-2-oxazoline) (PGE) with transformable side chains was synthesized and complexed with $H_3PW_{12}O_{40}$ (PW) by electrostatic self-assembly, forming PGE/PW nanocomposite membranes with bicontinuous nanostructures. After a subsequent PA-treatment of these membranes, high-temperature PEMs of PGE/PW/PA ternary nanocomposites were obtained, in which the *in situ* electrostatic crosslinking effect between PW and PGE side chains was generated in the hydrophilic domains of the bicontinuous structures. The microphase separation structure and the electrostatic crosslinking feature endow the PGE/PW/PA membranes with excellent anhydrous proton conductive ability while retaining high mechanical performance. The membranes show a high proton conductivity of 42.5 mS/cm at 150 °C and a high tensile strength of 13 MPa. Our strategy can pave a new route based on electrostatic control to design nanostructured polymer electrolytes.

Proton exchange membranes (PEMs) are the key components in fuel cells, which require both high proton conductivity and mechanical properties to achieve sufficient power density and safety [1,2]. Commercial perfluorosulfonic acid membranes (PFSAs) such as Nafion are the most widely used with excellent performance at low temperatures and high relative humidity (RH) [3,4]. However, PFSAs have relatively low glass transition temperatures and cannot establish a well-connected proton transport channel in the dry state, which leads to a dramatic decrease in mechanical stabilities and proton conductivity above 100 °C [5]. Therefore, it is urgent to develop PEMs with excellent performance at high temperatures. At present, the most practical PEM materials for high-temperature applications are phosphoric acid (PA)-doped polymer membranes [6–8]. Generally, such membranes require a high amount of PA adsorption to ensure proton conductivity. However, the large amount of PA reduces the mechanical strength of the membranes due to the plasticizing effect [9]. Thus, addressing the trade-off between proton conductivity and mechanical performance becomes the key issue for PA-doped PEMs.

Recently, researchers have focused on balancing the conductive and mechanical properties of PA-doped PEMs by crosslinking or microphase-separating strategies [10]. Crosslinking is performed by restricting the movement of polymer chain segments through covalent or non-covalent bonds to counteract the plasticizing effect of adsorbed PA, wherein small molecules, polymers and particles have been used as crosslinkers [11,12]. Although the mechanical strength can be substantially improved, a high crosslinking degree may make the material brittle. Constructing microphase structures in membranes is commonly employed in PEMs, which can reduce the proton transport energy barriers and realize efficient proton transport [13,14]. The microphase structure allows the PA to be selectively distributed only in the hydrophilic domains without disturbing the mechanically supporting domains. Besides, the mechanical strength of PEMs can also be effectively enhanced by nanofillers, such as inorganic nanoparticles and nanoclusters [15]. Among them, polyoxometalates as nanosized solid superacids have attracted much attention.

* Corresponding author.
E-mail address: hl_li@jlu.edu.cn (H. Li).

https://doi.org/10.1016/j.cclet.2022.05.011
1001-8417/

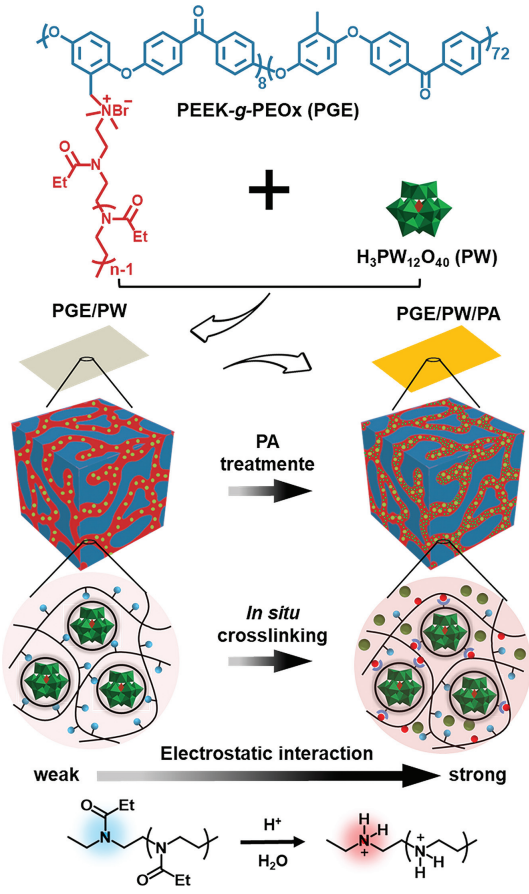

Fig. 1. Preparation strategy of POM-polymer nanocomposite PEMs.

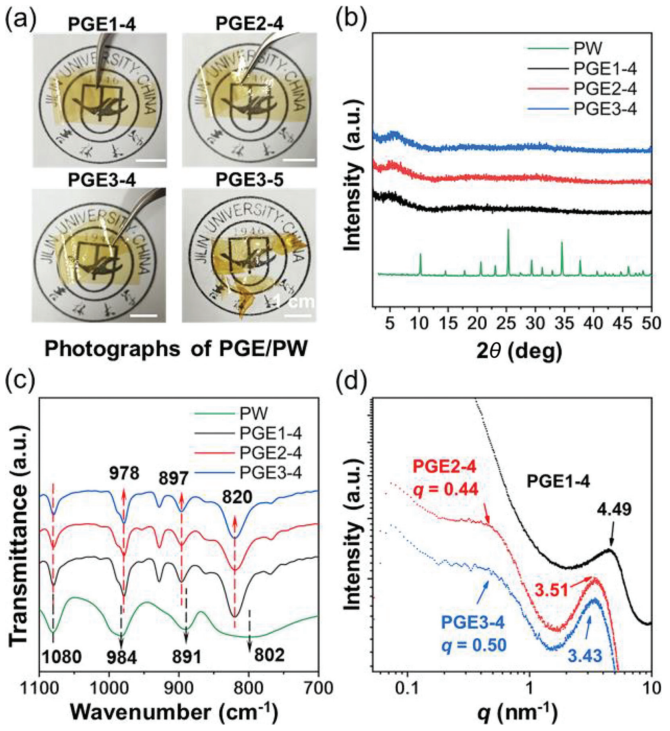

Fig. 2. (a) Photographs of PGE/PW nanocomposite membranes. (b) XRD patterns and (c) FTIR spectra of PW, PGE1–4, PGP2–4 and PGP3–4. (d) SAXS profiles of PGE1–4, PGE2–4 and PGE3–4.

Polyoxometalates (POMs), comprising a large class of ionic metal oxide nanoclusters with well-defined structures and uniform size [16–20], show abundant properties in the fields of catalysis, electrics, optics, *etc*. [21–25], and they were widely used to prepare hybrid nanocomposites [26–35]. Especially, POMs are suitable for use in high-temperature anhydrous environments due to their excellent water retention capacity, outstanding thermal stability, and high proton conductivity [36–48]. For example, our group recently reported a study of POM-based anhydrous liquid-crystalline electrolytes with high structural stability and high proton conductivity [49]. In addition, the characteristics of multivalent anions enable POMs as electrostatic crosslinkers to construct ionic self-assembled materials and achieve significant mechanical enhancement [50]. Thus, combining the advantages of POMs with microphase-separated polymer matrices is promising to develop high-performance PEMs for high-temperature proton conduction.

In this work, we constructed electrostatic crosslinked PA-doped PEMs with bicontinuous nanostructure based on POMs and comb copolymers (Fig. 1). The whole idea takes full account of the topological structure and mechanical strength of matrix polymers, as well as the noncovalent interaction between POMs and polymer moieties. We synthesized amphiphilic comb copolymers poly(ether-ether-ketone)-*grafted*-poly(2-ethyl-2-oxazoline) (PEEK-*g*-PEOx, which is abbreviated as PGE) with transformable side chains. The comb copolymer is easy to form well-connected nanostructures due to the aggregation of long hydrophilic side chains, in which PEEK as the main chain can impart mechanical stability, and PEOx side chains have weak electrostatic interactions with POMs and PA. Note that the hydrolysis of PEOx to polyethyleneimine (PEI) leads to strong electrostatic interactions with POMs and PA. Initially, flexible and transparent nanocomposite membranes with tunable bicontinuous structures were constructed by the electrostatic self-assembly of PGE with $H_3PW_{12}O_{40}$ (PW). Then, the membranes were treated by PA region-selective enrichment, in which the *in situ* electrostatic crosslinking between PW and PGE side chains was generated in the hydrophilic domains of the bicontinuous structure. As expected, the bicontinuous structure and the electrostatic crosslinking effect significantly improved the proton conductivity and the mechanical strength of the resultant membranes.

The comb copolymer PGE was synthesized by the "grafting to" method, in which optimized PEOx side chains (M_w of *ca.* 2000, PDI of *ca.* 1.09) obtained from ring-opening polymerization were attached to PEEK backbones (M_w of *ca.* 25,000, PDI of *ca.* 2.7) by nucleophilic substitution reaction. We obtained three comb copolymers PGE1, PGE2, and PGE3 with a certain graft length and increasing graft density of 0.05, 0.11 and 0.17, respectively. A more detailed synthesis process and characterization are shown in Figs. S1-S8 (Supporting information). A series of PGE/PW precursor membranes were prepared by a simple solution casting method, in which anhydrous solvents were used to prevent the inherent acidity of PW from hydrolyzing the amide groups of PEOx. The PGE/PW membrane was identified as PGEx-y, where x and y represent the polymer type and the PW content, respectively (*e.g.*, PGE3–4 means using PGE3 and the PW content of 40 wt%). Since a high PW content can make the membranes brittle or opaque (Fig. 2a and Fig. S9 in Supporting information), we optimized the maximum content of PW to be 40 wt%.

All PGE1–4, PGE2–4 and PGE3–4 samples were flexible and transparent (Fig. 2a), implying that the PW and PGE are compatible with each other. To further clarify the microscopic homogeneity, the membranes were measured by X-ray diffraction (XRD) (Fig. 2b). The XRD patterns of the nanocomposite membranes exhibited no characteristic peaks belonging to crystalline PW aggregates, which supports that PW clusters are homogeneously dispersed in the PGE polymer matrix. The interaction between the

PW and the PGE was further revealed by Fourier transform infrared spectroscopy (FTIR) (Fig. 2c). In the IR spectrum of pristine PW, four kinds of oxygen atoms in PW give rise to the characteristic vibration bands at 802 cm^{-1} ν_{as}(W–O_c–W), 891 cm^{-1} ν_{as}(W–O_b–W), 984 cm^{-1} ν_{as}(W=O_d), 1080 cm^{-1} ν_{as}(P–O_a). These vibration bands were all observed in the IR spectra of PGE1–4, PGE2–4, and PGE3–4, demonstrating the PW clusters remained structural integrity in the composites. Compared to pristine PW, slight shifts were noticed in these vibration bands for all three nanocomposites. The ν_{as}(W–O_b–W) and ν_{as}(W–O_c–W) peaks shifted to the high-frequency region, appearing at 897 and 820 cm^{-1}, whereas, the ν_{as}(W=O_d) peaks shifted to the low-frequency region, appearing at 978 cm^{-1}. The shift of characteristic peaks indicates that the chemical environment around PW has changed, which is recognized as the weak electrostatic interaction between the PW and the amide groups of PEOx, similar to the results reported in the literature [51,52].

The microscopic structures of PGE/PW composite membranes were investigated by using the small-angle X-ray scattering (SAXS) and transmission electron microscopy (TEM). The SAXS results displayed that PGE2–4 and PGE3–4 showed significant scattering peaks at the low q region of 0.44 nm^{-1} and 0.50 nm^{-1}, corresponding to d-spacing of about 14.3 nm and 12.6 nm calculated by the equation $d = 2\pi/q$, which indicated that both membranes had typical microphase-separated structures (Fig. 2d). The SAXS profile of PEG1–4 lacks the microphase signal due to the small volume fraction of its hydrophilic component that could not form well-defined microphase domains. It is noteworthy that the SAXS profiles show scattering peaks at 4.49 nm^{-1}, 3.51 nm^{-1}, and 3.43 nm^{-1} at the high q region for PGE1–4, PGE2–4, and PGE3–4, corresponding to d-spacing of 1.4 nm, 1.79 nm, and 1.83 nm, respectively. This set of scattering peaks reflects the distribution distance of PW in the polymer matrix, and the increasing d-spacing of PW with the PEOx domain sizes is due to the decreased distribution density of PW in the domains, which also reflects the uniform dispersing state of PW. TEM was used to further explore the microphase structure of the membranes. We prepared ultrathin sections of different PGE/PW membranes with a thickness of *ca.* 80 nm. The area containing PW is black in the bright-field model because the W element is more difficult to be penetrated by the electron beam. TEM images show that all three PGE/PW membranes form a network-like bicontinuous structure, in which the hydrophilic domain composed of PEOx/PW and the hydrophobic domain formed by PEEK are highly intertwined (Fig. 3). Notably, the three samples show varied bicontinuous structures although they load the same content of PW. As the grafting density of the comb copolymer matrix increases from PGE1–4, PGE2–4 to PGE3–4, their bicontinuous network becomes denser with smaller phase sizes, which exhibits higher connectivity of the PEOx/PW domain. This phenomenon is consistent with the decreased d-spacing in the SAXS results.

The PGE/PW/PA ternary PEMs were prepared by PA region-selective adsorption into the bicontinuous structure of PGE/PW membranes. The hydrophobic PEEK domains are incompatible with PA. In contrast, both components in the hydrophilic domains of PEOx/PW are capable of hydrogen bonding or electrostatic interacting with PA. Consequently, PA can selectively enrich the PEOx/PW, which results in a high local concentration of PA in the PEOx/PW domain despite the relatively small percentage of PA in the whole membranes, thus ensuring a high proton conductivity while retaining mechanical strength. The effect of PA-adsorption on the membrane performance was investigated by taking PGE3–4/PA as an example. The inset in Fig. 4a shows that PGE3–4/PA remains flexible and transparent after PA-treatment, and its SAXS profile also maintains the bicontinuous structure. The d-spacing of phase size increased from 12.6 nm for PGE3–4 to 14.0 nm for PGE3–4/PA, which should be attributed to the swelling of hydrophilic domains after

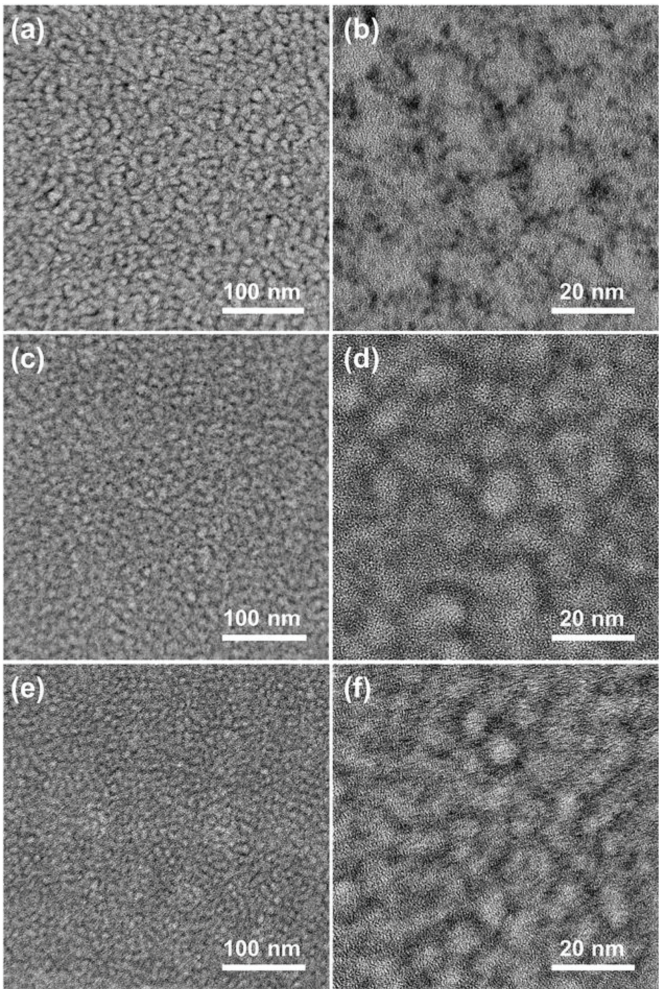

Fig. 3. Bright-field TEM images of the ultrathin microtomed sections of the PGE/PW nanocomposite membranes: (a, b) PGE1–4, (c, d) PGE2–4, (e, f) PGE3–4.

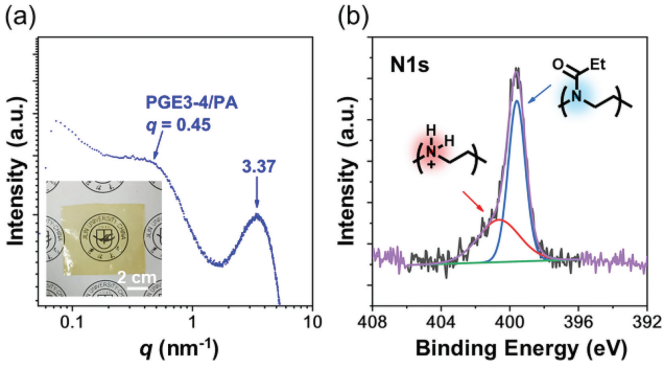

Fig. 4. (a) SAXS profile and (b) XPS spectrum of the PGE3–4/PA membrane. Inset of (a) is the photograph of this sample.

PA enrichment in. Meanwhile, the d-spacing of PW increases from 1.83 nm to 1.86 nm due to the dilution effect of PA (Fig. 4a). In addition, the PA-treatment process caused an *in situ* electrostatic crosslinking effect. PEOx chains were easily converted to PEI chains because of the acidic hydrolysis of the amide bond, resulting in the partial conversion of PEOx/PW domains to PEI/PW domains. PEI can offer a strong electrostatic crosslinking with the multi-charged PW, which immobilizes the ionic domains of the bicontinuous structure, suppresses membrane swelling, and thus enhances the mechanical properties.

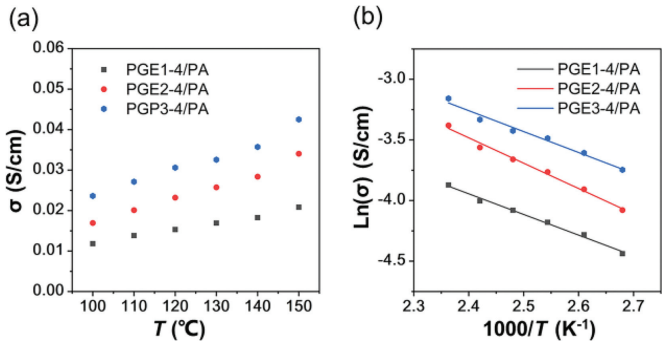

Fig. 5. (a) Temperature-dependent conductivities and (b) Arrhenius fitting of PGE1–4/PA, PGE2–4/PA and PGE3–4/PA from 100 °C to 150 °C.

Table 1
Summary of PGE/PW/PA nanocomposite membranes.

Sample	w_{PW} (%) [a]	x [b]	PA uptake (wt%)	σ (mS/cm) [c]
PGE1–4/PA	40	0.05	76	20.8
PGE2–4/PA	40	0.11	91	34.0
PGE3–4/PA	40	0.17	108	42.5

[a] Weight fraction of PW in the PGE/PW membranes.
[b] Grafting density of PEOx in PGE.
[c] Proton conductivity at 150 °C.

To confirm the electrostatic crosslinking effect, we tested the binding energy of N 1s electron in the PGE3–4/PA membrane using X-ray photoelectron spectroscopy (XPS). Fig. 4b shows that the membrane appears to have two types of N, which is considered the result of PEOx hydrolysis for the generation of PEI. The difference between the strong electrostatic interaction of PEI/PW and the weak electrostatic interaction of PEOx/PW can be clearly illustrated by an experiment to evaluate the complexation strength in aqueous solutions. PW remained soluble after mixing with the aqueous solution of PEOx, while a precipitate rapidly formed when mixing PW with the aqueous solution of PEI because of the strong electrostatic crosslinking between PW and PEI (Fig. S10 in Supporting information). Our *in situ* crosslinking strategy takes the advantage of the easy hydrolysis of PEOx and the good dispersibility of PW in PEOx components. The crosslinking degree can be easily regulated by varying the PW content, which can further control the amount of adsorbed PA as well as the mechanical and conductive properties.

The proton conductivities (σ) of PGE/PW/PA membranes were measured by AC impedance measurements in the temperature range of 100–150 °C (Fig. 5a and Table 1). The corresponding Nyquist plots are shown in Fig. S11 (Supporting information). The conductivities of PGE1–4/PA, PGE2–4/PA, and PGE3–4/PA at 150 °C are 20.8, 34.0 and 42.5 mS/cm, respectively. This tendency is consistent with their channel continuity. By Arrhenius fitting, the proton conduction activation energies (E_a) of PGE1–4/PA, PGE2–4/PA, and PGE3–4/PA are 0.14, 0.18, and 0.15 eV, respectively, proving that proton conduction in this anhydrous system is a Grotthuss conduction mechanism (Fig. 5b). The PW can assist the dissociation of PA molecules [53]. The synergetic conducting effect between PW and PA enhanced proton mobility, which endowed a high conductivity to the membranes at a low PA-upaking state. Among the three membranes, PGE3–4/PA behaved the best in conductivity. In addition, the PGE3–4/PA membrane shows a high tensile strength of 13.0 MPa.

Besides, we further investigate the reinforcing effect of PW on the mechanical stability of membranes by using PGE3/PW/PA system as an example. We found that the membranes were remarkably reinforced from PGE3/PA, PGE3–1/PA, PGE3–2/PA, PGE3–3/PA to PGE3–4/PA with maximum tensile strengths of 5.0, 7.5, 9.1, 10.7, 13.0 MPa (Fig. S12a in Supporting information). Moreover, their dimensional stability also increases with the increasing PW content (Fig. S12b in Supporting information). Not only because the bicontinuous network constructed by PW can significantly increase the mechanical properties but also because the strong electrostatic interaction between PW and PEI enhances the overall mechanical strength. Compared with other PA-doped PEMs reported in the literature, our membranes have obvious advantages in comprehensive performance (Table S1 in Supporting information).

In summary, we developed an *in situ* crosslinking strategy to construct robust high-temperature PEMs based on POM-polymer nanocomposites. A comb copolymer PGE with transformable side chains was synthesized and complexed with PW *via* electrostatic self-assembly, forming bicontinuous PGE/PW nanocomposite as precursor membranes. After a further PA-treatment, PGE/PW/PA PEMs were prepared by PA region-selective enrichment, in which the *in situ* electrostatic crosslinking effect between PW and PGE side chains was generated. The bicontinuous microphase structure and the electrostatic crosslinking feature enable the PGE/PW/PA membranes with both high anhydrous proton conductivity and high mechanical performance. The optimized membrane PGE3–4/PA shows a high proton conductivity of 42.5 mS/cm at 150 °C and outstanding tensile strength of 13 MPa. This approach can provide a new concept based on electrostatic control to design nanostructured polymer electrolytes.

Declaration of competing interest

The authors declare that they have no known competing financial interests or personal relationships that could have appeared to influence the work reported in this paper.

Acknowledgments

The authors acknowledge financial support from the National Natural Science Foundation of China (No. 22075097), the Program for JLU Science and Technology Innovative Research Team (No. 2017TD-10), and the Open Research Fund of State Key Laboratory of Polymer Physics and Chemistry, Changchun Institute of Applied Chemistry, Chinese Academy of Sciences (No. 2020–09).

Supplementary materials

Supplementary material associated with this article can be found, in the online version, at doi:10.1016/j.cclet.2022.05.011.

References

[1] K. Jiao, J. Xuan, Q. Du, et al., Nature 595 (2021) 361–369.
[2] N. Li, M.D. Guiver, Macromolecules 47 (2014) 2175–2198.
[3] Y. Li, Z. Li, W. Wang, et al., Sci. China Mater. 63 (2020) 1235–1246.
[4] B. Liu, B. Hu, J. Du, et al., Angew. Chem. Int. Ed. 60 (2021) 6076–6085.
[5] D.W. Shin, M.D. Guiver, Y.M. Lee, Chem. Rev. 117 (2017) 4759–4805.
[6] H. Tang, K. Geng, L. Wu, et al., Nat. Energy 7 (2022) 153–162.
[7] F. Liu, S. Wang, H. Chen, et al., Renew. Energ. 163 (2021) 1692–1700.
[8] J.A. Asensio, E.M. Sanchez, P. Gomez-Romero, Chem. Soc. Rev. 39 (2010) 3210–3239.
[9] Q. Li, J.O. Jensen, R.F. Savinell, et al., Prog. Polym. Sci. 34 (2009) 449–477.
[10] J. Dai, Y. Zhang, G. Wang, et al., Sci. China Mater. 65 (2021) 273–297.
[11] M. Zeng, H. Guo, G. Wang, et al., J. Colloid Interface Sci. 603 (2021) 408–417.
[12] P. Sun, Z. Li, S. Wang, et al., J. Membr. Sci. 549 (2018) 660–669.
[13] H. Bai, H. Wang, J. Zhang, et al., J. Membr. Sci. 592 (2019) 117395.
[14] L. Wang, Y. Wu, M. Fang, et al., J. Membr. Sci. 602 (2020) 117981.
[15] X.M. Li, L.Z. Dong, J. Liu, et al., Chem 6 (2020) 2272–2282.
[16] H. Liu, C.H. Hsu, Z. Lin, et al., J. Am. Chem. Soc. 136 (2014) 10691–10699.
[17] J. Tang, C. Ma, X.Y. Li, et al., Macromolecules 48 (2015) 2723–2730.
[18] H. Wei, J. Zhang, N. Shi, et al., Chem. Sci. 6 (2015) 7201–7205.
[19] S. Chai, X. Cao, F. Xu, et al., ACS Nano 13 (2019) 7135–7145.
[20] S.C. Chai, T.Y. Xu, X. Cao, et al., Chin. J. Polym. Sci. 37 (2019) 797–805.
[21] J. Zhou, T. Yu, K. Li, et al., Inorg. Chem. 61 (2022) 3050–3057.
[22] K. Li, X.L. Lin, K. Zeng, et al., Tungsten 4 (2022) 149–157.
[23] X. Chen, G. Zhang, B. Li, et al., Sci. Adv. 7 (2021) eabf8413.

[24] H. Li, S. Pang, S. Wu, et al., J. Am. Chem. Soc. 133 (2011) 9423–9429.
[25] H. Li, W. Qi, W. Li, et al., Adv. Mater. 17 (2005) 2688–2692.
[26] H. Li, L. Wu, Polym. Int. 69 (2019) 665–667.
[27] J. Zhang, Z. Miao, J. Yan, et al., Macromol. Rapid. Commun. 40 (2019) 1800730.
[28] Q. Liu, X. Wang, Matter 2 (2020) 816–841.
[29] J. Luo, X. Sun, J.F. Yin, et al., Giant 2 (2020) 100013.
[30] L.J. Ren, H.K. Liu, H. Wu, et al., Adv. Mater. 32 (2020) 1805863.
[31] T. Wen, L. Qiu, Z. Zheng, et al., Macromolecules 53 (2020) 1415–1421.
[32] J. Xiao, Q. He, S. Qiu, et al., Sci. China Chem. 63 (2020) 792–801.
[33] Y. Cui, L. Yin, X. Sun, et al., ACS Appl. Mater. Interfaces 13 (2021) 47155–47162.
[34] H. Bian, X. Zhang, H. Zhao, et al., Chin. Chem. Lett. 30 (2019) 1097–1099.
[35] G. Hu, W. Chang, S. An, et al., Chin. Chem. Lett. 33 (2022) 3968–3972.
[36] Y. Liu, S. Liu, X. Lai, et al., Adv. Funct. Mater. 25 (2015) 4480–4485.
[37] J.C. Liu, Q. Han, L.J. Chen, et al., Angew. Chem. Int. Ed. 57 (2018) 8416–8420.
[38] H. Wu, X. Wu, Q. Wu, et al., Compos. Sci. Technol. 162 (2018) 1–6.
[39] T. Iwano, S. Miyazawa, R. Osuga, et al., Commun. Chem. 2 (2019) 1–8.
[40] M. Zhang, A.M. Zhang, Y. Chen, et al., Energy Storage Mater 29 (2020) 172–181.
[41] S. Li, Y. Zhao, S. Knoll, et al., Angew. Chem. Int. Ed. 60 (2021) 16953–16957.
[42] L. Liu, Z. Wu, Z. Zheng, et al., Chin. Chem. Lett. 33 (2022) 4326–4330.
[43] X. Sun, S. Liu, Q. Wu, et al., Inorg. Chem. Front. 8 (2021) 3149–3155.
[44] L. Zhai, H. Li, Molecules 24 (2019) 3425.
[45] L. Zhai, S. Chai, G. Wang, et al., Macromol. Rapid. Commun. 41 (2020) 2000438.
[46] H. He, G. Wang, S. Chai, et al., Chin. Chem. Lett. 32 (2021) 2013–2016.
[47] H. Guo, M. Zeng, X. Li, et al., ACS Appl. Mater. Interfaces 13 (2021) 30039–30050.
[48] X. Li, H. Zhao, Y. Li, et al., Chin. Chem. Lett. 33 (2022) 4675–4678.
[49] S. Chai, F. Xu, R. Zhang, et al., J. Am. Chem. Soc. 143 (2021) 21433–21442.
[50] L. Zhang, T. Cui, X. Cao, et al., Angew. Chem. Int. Ed. 56 (2017) 9013–9017.
[51] J. Chen, X. Fang, X. Duan, et al., Green Chem. 16 (2014) 294–302.
[52] G. Wang, J. Li, L. Shang, et al., CCS Chem. 4 (2022) 151–161.
[53] J. Zhang, S. Chen, H. Bai, et al., Int. J. Hydrogen Energy 46 (2021) 11104–11114.